MANIPULATION

Embodied manipulation with past and future morphologies through an open parametric hand design

Kieran Gilday[1]*, Chapa Sirithunge[2], Fumiya Iida[2], Josie Hughes[1]

A human-shaped robotic hand offers unparalleled versatility and fine motor skills, enabling it to perform a broad spectrum of tasks with precision, power, and robustness. Across the paleontological record and animal kingdom, we see a wide range of alternative hand and actuation designs. Understanding the morphological design space and the resulting emergent behaviors can not only aid our understanding of dexterous manipulation and its evolution but also assist with design optimization, achieving and ultimately surpassing human capabilities. Exploration of hand embodiment has, to date, been limited by challenges of accessibility in customizable hands in the real world and by the reality gap in simulation of complex interactions. We introduce an open parametric design that integrates techniques for simplified customization, fabrication, and control with design features to maximize behavioral diversity. Nonlinear rolling joints, anatomical tendon routing, and a low–degree-of-freedom modulating actuation system enable rapid production of single-piece 3D-printable hands without compromising dexterous behaviors. To demonstrate this, we evaluated the low-level behavior range and stability of the design, showing variable stiffness over two orders of magnitude. In addition, we fabricated three hand designs: human, mirrored human with two thumbs, and aye-aye hands. Manipulation tests evaluated the variation in each hand's proficiency at handling diverse objects and demonstrated emergent behaviors unique to each design. Overall, we introduce diverse designs for robotic hands, provide a design space to compare and contrast different hand morphologies and structural configurations, and share a practical and open-source design for investigating embodied manipulation.

INTRODUCTION

The capabilities of the human hand performing robust and diverse behaviors arises through synergistic interactions between the brain and body (*1*–*3*), demonstrating the fundamental principle of embodied intelligence (EI), that cognition is deeply rooted in the body's interactions with the world (*4*, *5*). Specifically for the hand, EI describes the synergy between the capabilities of the brain, the control of actuators or muscles, and the body, the hand morphology, and passive properties of the hand. For a given environment or required task space, animals exploit their actuation and control to achieve complex motions with a finite set of actuators, whereas the morphology and passivity provide physical robustness and behavioral diversity through local processing of physical stimuli. For example, the human hand is highly specialized for precision gripping and fine motor tasks, whereas the chimpanzee hand, adapted for climbing and brachiation, features longer, more curved fingers and shorter thumbs, optimizing it for holding strength but limiting precision (*6*). Furthermore, hand structure and functionality undergo substantial changes throughout growth and development. During this period, the human hand experiences enhancement in grip strength and stability, transitioning from exploration in childhood to refined, complex use in adulthood (*7*). Understanding the interplay among hand morphology, passive nonlinearity, and synergistic actuation (*8*–*10*) would provide a greater understanding of the contribution of EI and how to design these properties for given task or environment.

Exploring a wide range of hand embodiments requires a structured and scalable approach to design customization and evaluation. Simulation is one tool that could overcome the fabrication and scaling bottleneck (*11*, *12*). However, physics simulators are still limited in their ability to capture nuanced contact forces or multimaterial interactions (*13*, *14*). Thus, it remains fundamental to develop a design space for complex hands that can be fabricated and controlled in the real world while maintaining their passive emergent properties. To date, the design of dexterous robotic hands has largely focused on bioinspired hands, which mimic the morphology of human hands to achieve similar emergent and robust capabilities (*1*, *2*, *15*–*17*). There have been many anthropomorphic hands that closely mimic the human hand bone structure and tendon routing (*16*–*21*), resulting in adaptive behaviors (*18*), high performance (*19*), dexterity (*16*, *17*), and emergent grasping (*21*). Furthermore, soft robotic principles have been integrated to great success in the RBO Hand 3 (*2*), Pisa/IIT SoftHand (*22*, *23*), and the ADAPT Hand (*24*). For example, the introduction of compliance and underactuation provides robustness in open-loop in-hand manipulation (*2*) and generation of synergistic pinching and grasping behaviors with only one– to two–degrees-of-freedom actuation (*22*). Maintaining these state-of-the-art hand properties of performance, dexterity, and robust behaviors within a customizable and accessible design is essential for large-scale design space exploration.

Bespoke and customizable robotic hands have been gaining traction. Personalized prosthetics and task-specific body-controller codesign, in particular, have seen increasing popularity enabled by increasing accessibility and capabilities of rapid prototyping, 3D printing technologies (*25*–*30*). Customizable designs often leverage living hinge joints such that they can be printed with a single material and require minimal assembly or postprocessing (*28*, *31*). However, these typically have poor behavioral diversity because the in-built joint stiffness and force range are restricted by flexure joint properties and interactions are limited by underactuated and nonreconfigurable tendon routing (*28*, *32*). Other designs use more complex rolling joints or multimaterial 3D printing to achieve greater behavioral diversity

[1]CREATE Lab, Department of Mechanical Engineering, Swiss Federal Institute of Technology in Lausanne, Lausanne, Switzerland. [2]Bio-Inspired Robotics Lab, Department of Engineering, University of Cambridge, Cambridge, UK.
*Corresponding author. Email: kieran.gilday@epfl.ch

(*26*, *33*–*35*). However, these designs often remain highly integrated and complex to fabricate (*25*, *36*). In addition, these designs often overconstrain joints, reducing compliance and potentially limiting emergent behaviors and resilience (*23*). Parametric and modular designs offer the most potential for customization (*27*, *31*, *37*–*39*). However, as with previous flexure hands, the ability of existing parametric designs to encode diverse behaviors is limited by their low number of parameters and morphological simplifications made to the joint, tendon, and actuation design (*31*, *40*–*42*). Overall, existing hands show many trade-offs; for example, biomimetic or soft manipulation hands show high performance but lack customization because of their high complexity (*2*, *18*), customizable hands that can easily be optimized but exhibit limited behavior ranges with constrained actuation, or 3D printable prosthetics for accessibility at the cost of performance in dexterity and payload (table S1).

To address the limited encoding capacity for morphological and behavioral diversity with scalability, we hypothesize that, through nonlinear joints, four interconnected degrees of freedom (DoFs) per finger, and modulation of tendon stiffness and tension, the performance and adaptability of state-of-the-art robotic hands (*2*, *21*, *23*) are preserved over a wide morphological design space and can be tuned for performance in different niches (Fig. 1). In addition, we propose a structure of this design space, inspired by both evolutionary and developmental processes, with sufficient room to describe futuristic, artificially evolved hands or expertly crafted, augmented hands. Figure 2A highlights two axes and a number of examples centered around the baseline: a full-scale human-like design. One axis corresponds to long-timescale changes in hand morphology, including evolutionary and data-driven processes driving hand designs toward different environmental niches. The second axis considers short-timescale deviations from the baseline, on one side natural growth and on the other artificial development, augmentation (*43*), and designs with no biological basis through expert-led or generative design. Successful navigation of this space requires a design that captures an individual hand's behavioral diversity in addition to variations in behaviors seen across different morphologies. These arise from high-dimensional interactions with subtle differences in relative finger properties and dimensions (*44*, *45*). With a structured design space and capable baseline hand design, opportunities are opened for future research from paleomimetics—studying the evolution of manipulation behaviors (*46*)—to generative and codesign developing hands for previously unidentified applications (*47*, *48*).

Here, we present our contributions to the design, actuation, and exploration of accessible embodied robotic hands. First, we share the open source, 56+ parameter design and characterization results that demonstrate how the underlying design approach of dislocatable and rolling joints, paired with 26 reconfigurable, anatomical tendons, enables diverse and accessible hands with stable joint behaviors and robustness when manufacturing with 3D printing. Second, we demonstrate the baseline performance of the open parametric hand (OPH) by comparing a human hand OPH to human data for reachability, grasping workspace, and range of interactions. For example, we see that the OPH achieves all 33

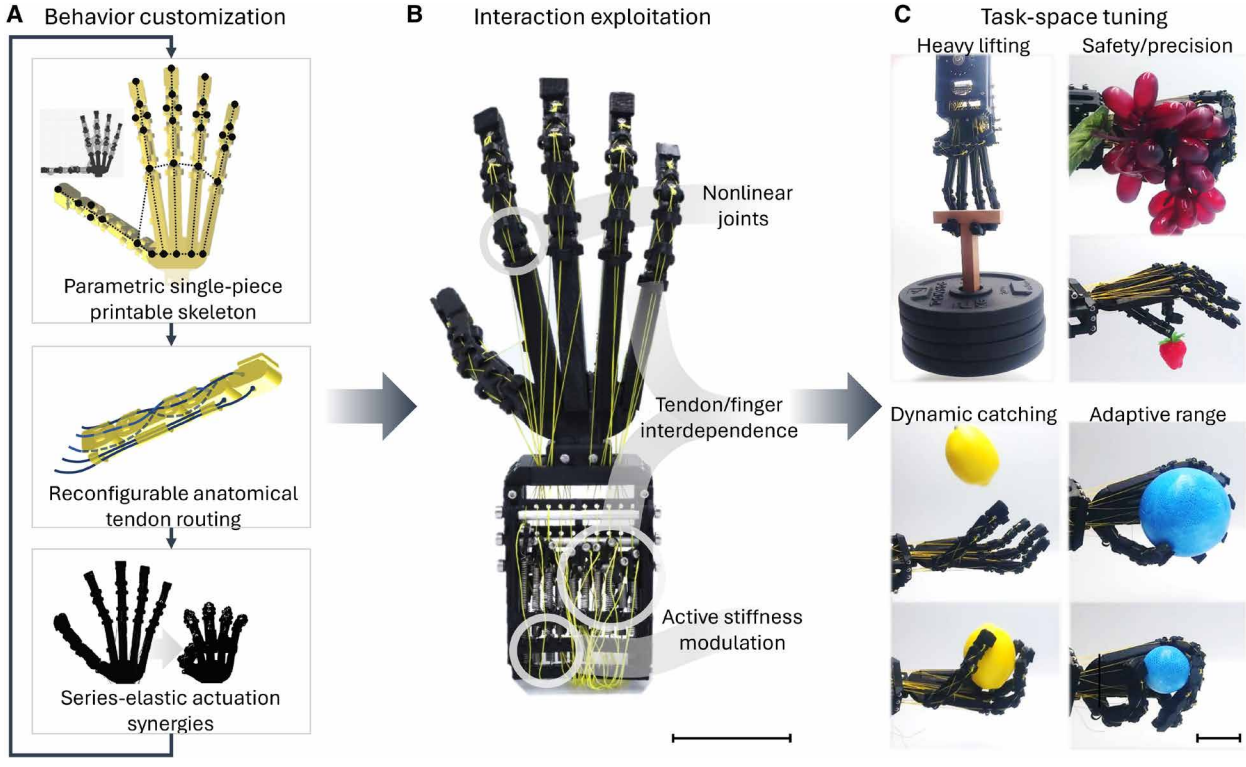

Fig. 1. Open parametric design for accessible, behaviorally diverse, functional hands. (**A**) Using single-piece 3D printing with parametric design, anatomical tendon routing/joints, and low-DoF synergistic actuation hands can be rapidly customized to suit a variety of tasks. (**B**) Hand behavioral diversity expands task capabilities and emerges from complex interactions between the nonlinear joints, tendon transmissions/joint coupling effects, and modulation of these by actuators (scale bar, 50 mm). (**C**) Functionality from accessible design/manufacturing, practical uses with high strength/capabilities in a variety of tasks, and minimal actuation (scale bar, 50 mm).

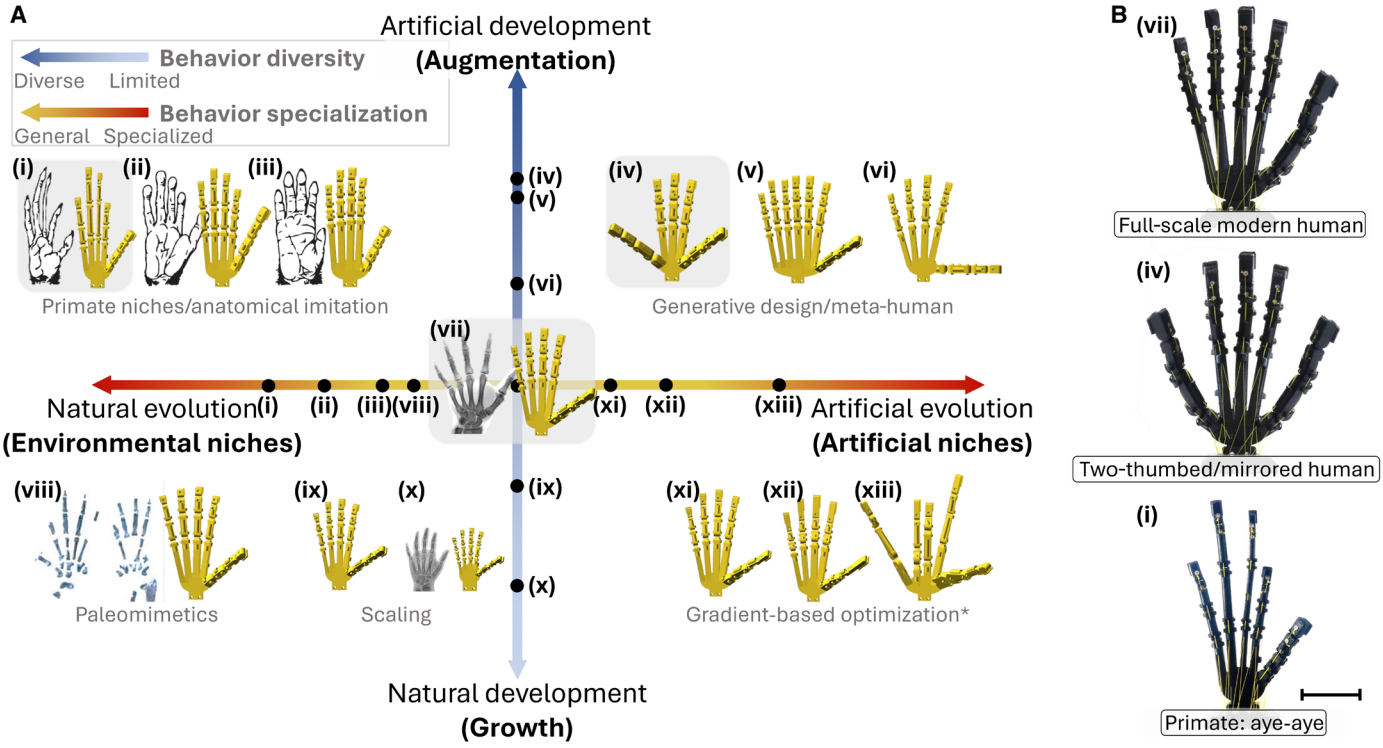

Fig. 2. Proposed design space requiring hands that can capture morphological and behavioral variations. (**A**) Exploration of embodied manipulation in two axes. Short-term development corresponds to the gain of behaviors via growth or augmentation. Long-term development corresponds to optimization within a particular niche. (i) Aye-aye; (ii) bush baby; (iii) chimpanzee [primate sketches from (*62*)]; (iv) mirrored/two-thumbed; (v) seven-fingered; (vi) flat human; (vii) baseline adult human; (viii) early hominid (4.4 million years ago) *Ardipithecus ramidus* [image of bones from (*61*)]; (ix) 75% scale human; (x) 50% scale human; (xi) to (xiii) theoretical hands optimized for human-like niches—nonhuman-like niches. (**B**) Highlighted human, aye-aye, and two-thumbed/mirrored hands were fabricated, testing behavioral diversity in the hand and behavioral variations across morphologies.

GRASP taxonomy human grasping types (*49*) and modulation of passive stiffness range up to 660%. Third, we introduce three actuation system configurations using one or two actuators driving customizable synergies and functional grasping behaviors to address the challenges of scalably actuating the hands. Last, we integrate the passive design and modular actuation in three designs representing different areas of the morphological design space. These include the human hand, a mirrored hand with two thumbs, and an aye-aye (a long-fingered primate) hand (Fig. 2B). Through performance metrics and highlights of unique manipulations (80-N weight lifting and writing with the human design, multiobject grasping with the mirrored design, and arboreal locomotion and foraging with the aye-aye design), we demonstrate that the OPH is capable of generating useful, varied, and tunable behaviors across the proposed design space. Overall, the interplay among our parametric encoding, joint design, and reconfigurable actuation results in a hand greater than the sum of its parts. With unique capacity for customization, accessible manufacturing, behavioral stability, and diversity, we broaden possibilities in the research of dexterous manipulation and its evolutionary and developmental underpinnings (*44*, *46*, *50*). This has further implications for applied robotic grasping, addressing needs of flexibility and customizability in task-optimized manipulation solutions (*12*, *48*, *51*–*53*), prosthetic devices (*54*, *55*), and meta-human augmentation (*43*).

RESULTS

The OPH combined key technologies of parametric, nonlinear joint design, anatomical tendon arrangement, and series elastic actuation synergies (Fig. 1). This enabled the encoding of a diverse range of manipulation behaviors and fabrication that is accessible (Fig. 1). To explore the morphological design space of the OPH, we focused on three hands: the full-scale modern human hand, a scaled up aye-aye hand, and a human hand augmented with a second thumb (Fig. 2B and movie S1). The aye-aye is a small primate whose hands are specialized for climbing and foraging for insects inside tree trunks (*56*). The aye-aye's hand morphology differs substantially in bone width, length, and joint diameters, with the middle finger equivalent in width and thickness to an ≈50% scale human hand (Fig. 2Ax). The design with two thumbs essentially mirrors the human design about the middle finger and we used this to highlight the potential for meta-human manipulation behaviors and the ability to customize beyond traditional anthropomorphism (*43*, *57*).

OPH design

The OPH parameterization makes a wide design space tractable while providing a wide range of designs over which joint behaviors remain stable. The hand can also be fabricated through single-piece 3D printing using consumer-grade printers, making it readily accessible. In the following section, we present our findings on defining a stable parameterization and operating within practical constraints.

Tractable, hierarchical, and parametric design

The OPH parameterization was chosen to simplify the design complexity while ensuring that the parameters encode critical and diverse behaviors. Figure 3A presents the design and principles of the OPH, and Fig. 3B highlights the most critical parameters.

At the foundation of the design hierarchy, Fig. 3A, is the rolling contact joint, which is partially constrained by a pair of flexure ligaments mimicking the collateral ligaments of human synovial joints (*58*). This joint is printable in a single piece and offers low friction and resilience to impacts. Joints are combined into bones with tendon paths and anchor points. Tendons are routed through static constraints and mimic the layout and function of tendon pulleys in biological hands (*19*, *59*). The fingers and thumb combine three joints [metacarpophalangeal (MCP), proximal interphalangeal (PIP), and distal interphalangeal (DIP)] and four bones (metacarpal, proximal, intermediate, and distal) into a modular design that has four DoFs driven by five tendons (extensor, abductor, adductor, intermediate flexor, and distal flexor), each affecting a minimum of two joints. These modular fingers can be combined into full hands, where four fingers and a thumb form a hand connected by a rigid palm. In human anatomy, the thumb is differentiated from the other fingers with additional motion in the second joint and intrinsic palmar muscles for greater abduction and opposition forces (*60*). Similarly, we include a sixth opposition tendon in the thumb (Fig. 3A).

At each level in the design hierarchy, we reduced the dimensionality of the design space by fixing parameters that are critical to behaviors and removing or combining those less critical. Figure 3B outlines these. At the joint level, diameter has the greatest influence on behaviors. Although the design space includes multiple joint types for sake of modularity, in almost all cases, joint type is fixed by finger design: PIP and DIP have constraints to reduce hyperextension, and the MCP is rounded to allow for control of abduction/adduction. Ligament thickness and width have minor impacts on behaviors; however, their minimum values were determined by manufacturing limits. One layer higher in the hierarchy is the bone parameters, including length, width, and pulley properties. Bone length and width are

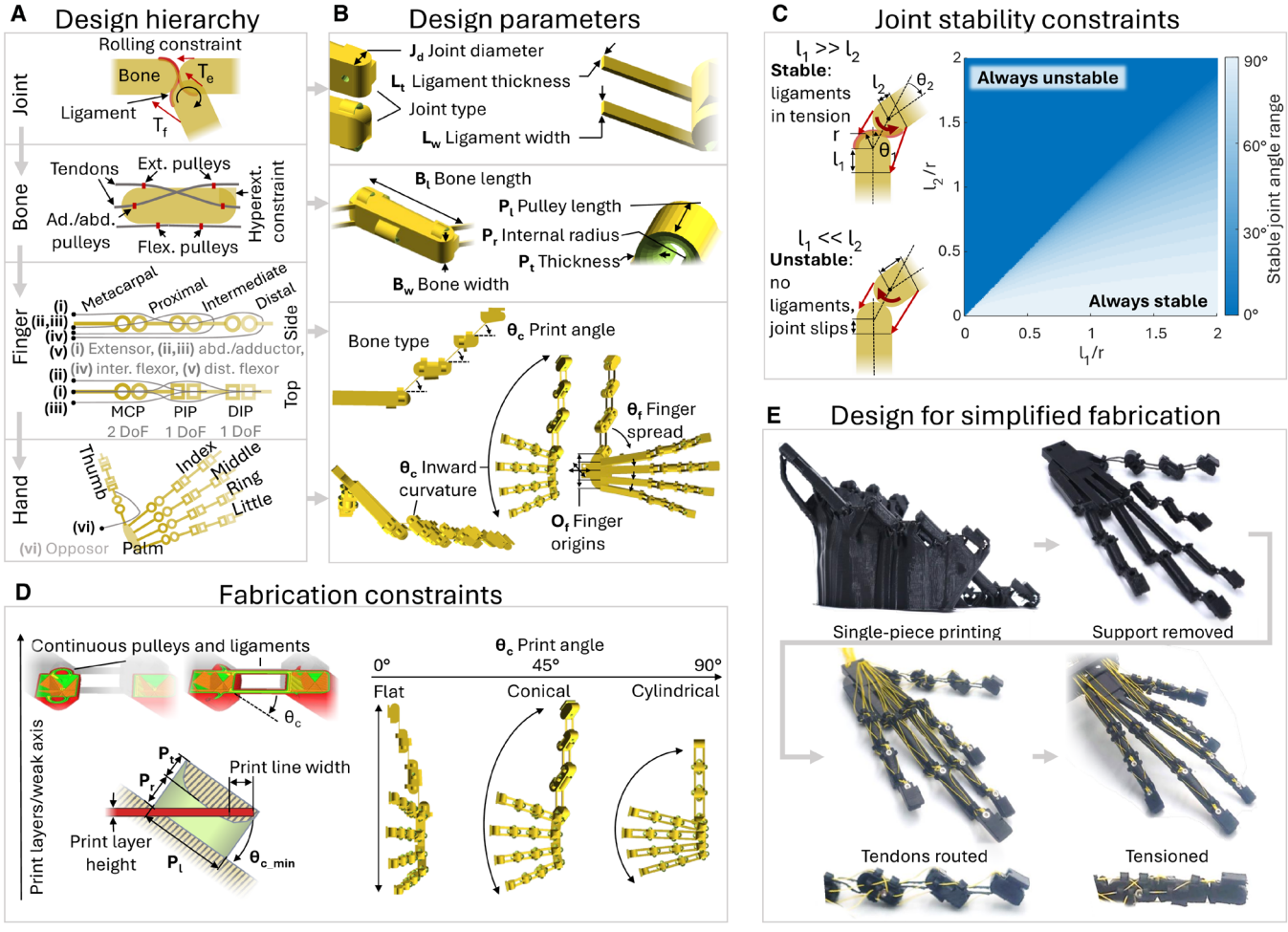

Fig. 3. Parametric design for emerging complexity with stable behaviors and single-piece 3D printing capabilities. (**A**) Single-ligament, nonlinear, rolling contact joints assembled into bones, then fingers, and then hands. (**B**) Highly customizable parameters from low-level joint parameters for stiffness/strength/range to high-level finger shapes and distributions for workspace and dexterity. (**C**) Joint design constraints. To prevent joint slipping, net tensile force should be sustained in ligament. With relative pulley placements $l_1 \gg l_2$, the joint is less likely to slip (stable). (**D**) Additive manufacturing defects minimized in printing plane, thereby constraining relative finger alignment and print angle. (**E**) 3D printing example: single-piece print process with support material, tendon routing, and then tendon pre-tensioning for regular joint operation.

strongly coupled to hand behaviors; however, width primarily influences only abduction/adduction, so we simplified this to one parameter per finger, the bone width. Pulley parameters are independent of behaviors and are determined by manufacturing constraints and strength requirements. Pulley placement, however, is critical for joint stability and defining the tendon arrangement. In Fig. 3C, we modeled the placement of the flexor tendon pulleys and chose fixed placement ratios relative to the joint radii ($l_1 = 1.5r$ and $l_2 = r$) that ensured that tendons pull the joint into stable conditions after dislocation; that is, with the second pulley placed further from the joint than the first pulley the ligaments experience compressive forces in more bone positions, which they cannot resist, and the joint dislocates. Always stable means that, even in the 90° dislocated position, the ligaments experience tension. Next, the finger consists of four of the same bone types defining motion axes and tendon arrangement. Finger placement is parameterized by translation of each finger origin, the relative spread of each finger (rotation in axis perpendicular to the palm), and a global curvature/print angle that defines the inward rotation of fingers toward each other.

With this parameterization and ignoring those fixed by tendon layout and joint stability, the OPH has three parameters per joint (one encoding and two practical), four per bone (one encoding and three practical), five per finger (all encoding), and one global (table S2). This gives a total of 151 parameters for a five-fingered hand. In practice, we treat pulley and ligament parameters globally, reducing the parameters to 66. Simplifying finger origins to translation in one dimension enables a further reduction to only 56 parameters. By varying only these parameters, we generated the morphological changes seen in Fig. 2A, from modern human hands to early hominid (*61*) and primate hands (*62*). Designs with different numbers of fingers and thumbs can be generated, and the number of parameters adapts accordingly.

Not all design parameters must be varied depending on the application and chosen method for design space exploration. Different methods for exploration include guided design using data and analysis of existing hands, such as primates and Napier indices (*45*), thereby varying few parameters to create hybrid hands with hybrid functionalities; generative design from large knowledge bases such as large language models for guided design iteration (*47*); landmark extraction using hand recognition algorithms and real-world hands (*63*), inferring unknowns in joint, pulley, and metacarpal parameters; and optimization algorithms with different sets of parameters and objective functions (fig. S2).

Design and manufacturing constraints

To ensure manufacturability and functional behaviors, we imposed constraints on a subset of the parameters. As mentioned, pulley placements were constrained for stable joint behaviors (Fig. 3C). A second constraint originated from the anisotropy introduced by layer-based 3D printing. For maximum strength, we oriented ligaments and pulleys to be in the printing plane. Figure 3D shows this constraint as a dependency on relative angles between fingers, hence a single global print angle/inward curvature parameter (Fig. 3B). This angle was then further constrained to $<\theta_{c\_min}$, depending on pulley dimensions to ensure continuity in at least one print layer.

Ligaments were printed extended and angled outward. After printing and once tension is applied, the joints naturally seat themselves in the correct position (movie S2). Figure 3E shows the printing and fabrication example of the aye-aye hand (Fig. 2B). After printing in a single piece, the tendons were fastened to their respective bone anchor points with bolts and routed through pulleys in the hand and palm to their actuation anchors.

Baseline passive hand performance

The OPH is a complex system with nonlinear joints, 20 DoFs, and 26 tendons. In the following section, we characterize the performance of the baseline design—with parameters taken from human skeletal data—by contrasting it with a real human. We used established metrics from the literature and some other key metrics that have been designed to capture the behavioral diversity of the hand and its ability to encode a range of different behaviors. To isolate the effects of morphology on the baseline capabilities, we only considered ranges of passive behaviors in the absence of active control. This was performed by connecting the tendons to passive springs.

Passive finger behaviors

First, we validated the baseline joints' range of motion (RoM) performance relative to human data. The range in Fig. 4A was measured by connecting tendons to passive springs, varying relative tendon length,s and recording the maximum joint angle configurations that could be held by the force equilibrium of the springs. The individual RoM of each joint was similar to that of a human (table S3), particularly so for the PIP joint and abduction axis of the MCP joint (*9*). The OPH had greater RoM in the DIP and MCP joints. However, overall, there was a reduction in the OPH RoM near the extended posture because of force coupling in the common tendons over the MCP and DIP joints, limiting simultaneous hyperextension and flexion in the absence of external forces. Nonlinearities and joint compliance can extend the RoM. For example, if the DIP is preflexed, the increased flexor tendon moment arm can prevent extension whereas the extensor tendon hyperextends the MCP. External forces can further decouple joint forces, allowing a wider RoM in stable equilibrium. In addition, external forces can cause dislocation, going beyond reported joint limits.

In Fig. 4B, the RoM was extrapolated into a reachability map (*64*) for a whole hand, with the OPH and human data scaled by finger length. Despite the variation in Fig. 4A RoM and increased human thumb abduction/adduction, the total reachability map volumes (calculated by the union of all fingers) were within 5% of each other (table S4). We also observed the intersection between the three volumes of index, middle, and thumbs as an indicator of the precision manipulation capabilities (*65*, *66*). Here, the OPH was lower by 43% because of the lower thumb abduction RoM.

For a third test, we characterized the emerging finger stiffness properties as a result of interacting bones, tendons, ligaments, and external stimuli, mirroring the complex behaviors observed in human fingers. We measured the force/displacement of the human design index finger for different test axes (fig. S4), starting finger poses, and passive spring stiffness configurations (Fig. 4C and movie S3). Figure 4Ci/ii shows the stiffness characteristics in the abduction test axis. The finger was probed laterally in the extended finger pose (black) and with the MCP flexed by 90° (blue), with two different spring configurations and pre-tension tuned to maintain each finger starting posture. The first configuration (fig. S5) was low stiffness with 0.11 N/mm for the abductor and adductor and 0.32 N/mm for the extensor and flexor springs (solid lines), and the second had higher stiffness [0.32 or 0.87 N/mm (dashed lines)]. The initial extension was dominated by static friction. After this, there was an approximately linear region of stiffness, and as expected, the stiffer spring configuration generated higher finger forces in both postures.

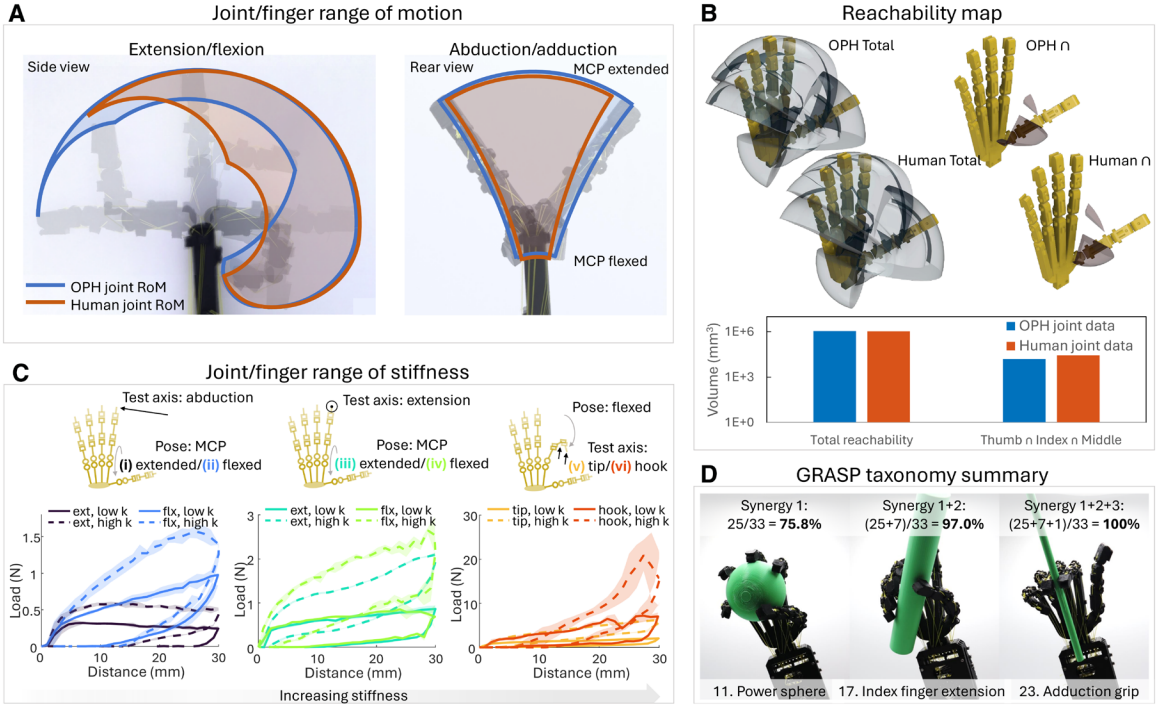

Fig. 4. Baseline passive behaviors. (**A**) Measured joint angle and finger ROM compared with human data. (**B**) Reachability maps and thumb/index/middle intersection (*65*) extrapolated to a whole hand for OPH and human data. (**C**) Joint/finger stiffness (*k*) range with varying test axes (three line graphs), start pose, and spring stiffness (solid and dotted lines) (mean and SD, $n = 3$). Single-variable stiffness change up to 290%, multivariable up to 660%. Finger starting poses controlled by varying relative tendon lengths. (**D**) Three of the 33 GRASP taxonomy grasp types (*49*) completed with three tendon configurations (all 33 possible types are shown in fig. S3).

Higher stiffness was seen in the MCP flexed posture; this follows the reduced abduction RoM seen in Fig. 4A. The changing joint contact alters the relationship between tendon force and joint rotation.

In the extension axis with the finger in the extended or MCP flexed position (Fig. 4Ciii/iv), the change in posture (dark to light green line) had a lesser effect than the change in spring configuration (dotted line). An increase in stiffness was observed because of the larger moment angle when the MCP was flexed. Higher stiffness was observed in this axis compared with abduction, despite the force acting in plane with all three joints, with peak forces approximately doubled.

Two final stiffness tests were performed with the finger in an approximately two-thirds flexed state (MCP, PIP, and DIP angles of 45°, 90°, and 45°, respectively) and probed at the fingertip (orange) in the extension axis and at the DIP (red) in the extension axis where a hook shape is formed (Fig. 4Cv/vi). The extension axis at the flexed fingertip behaved similarly to the extended and MCP flexed test, although with higher stiffness because of the mechanical advantage of the probe location closer to the MCP joint. The hook test behaved uniquely, with stiffness increasing with extension. This is due to joint coupling causing a blocking effect where the DIP flexes and conforms to the external geometry in response to MCP extension.

Observing the changes in mean stiffness across test axes, postures, and spring configurations, we saw the lowest change of 130% (≈0 to 280%) when varying finger posture between MCP extended and flexed. A change in the spring configuration gave the next highest change: 160% (≈60 to 220%). Last, a change in the test axis showed the highest change: ≈180% (≈−20 to 290%). Across all configurations, we saw a stiffness change of nearly two orders of magnitude by 660% (mean stiffness from 0.0086 to 0.65 N/mm). This is necessary for behavioral diversity and can be compared with the range of stiffness seen in human hands. Previous investigations have shown human finger passive stiffness in the range from 0.76 to 2.50 N/mm (*67*) (ellipsoid in the flex plane), mimicked by variable impedance actuators (*68*). Other results give a stiffness of 0.3 to 3 N/mm depending on applied forces (0.1 to 0.6 N/mm in just abduction) (*69*). This is between 230% in a single axis and 900% when exciting the finger with different forces. Although the index finger configurations that we tested show lower maximum stiffness (0.65 N/mm), the stiffness ranges showed a similar variation (200 to 660%).

In the final baseline test with the human OPH, we evaluated the useful workspace and conformability with the GRASP taxonomy (*49*). Figure 4D shows the results, where all 33 grasp types were achieved. The test was performed by attempting each grasp type in the default configuration (fig. S5) and then modifying the configuration and attempting any previous failed grasp types; these steps were repeated until all 33 were achieved. The first configuration/synergy successfully formed 25 grasp types, a second formed seven of the remaining eight, and a final synergy formed the last (full taxonomy and synergies described in fig. S3 with objects used in table S5). With a similar reachability to a human hand (Fig. 4B), we expected similar performance in this taxonomy. The ability to form each type with just three synergies highlights the robustness and adaptability of the baseline design.

Encoding finger behaviors

To leverage the OPH for applications requiring a customizable hand, the OPH must provide stable operation even with extreme parameter variation and show the ability to encode behaviors across different morphologies. The following results characterize behaviors of

representative fingers from the aye-aye and mirrored hand designs. Generated by measuring a real human's hand and sketches of aye-aye's (fig. S1) and then scaling to the same palm–to–index fingertip length, the three hands showed substantial variations in joint design, bone aspect ratios, and finger placements. We performed the same variable stiffness characterization as on the human OPH index finger (Fig. 4C) with the thumb of the mirrored design and the middle finger of the aye-aye.

For the minimum and maximum stiffness poses and test axes seen in Fig. 4C, stiffness was measured with the same spring configurations. Mean stiffness was calculated from the final load and displacement; the rise and plateau were calculated from lines fit to the first 5 mm and last 25 mm of displacement, respectively, which isolates the initial static friction phases and the spring-dominated phase.

Relative to the baseline design index finger, the mirrored design thumb was shorter by 15% and has 9% larger joint diameters, giving it mechanical advantage in transmitting force. In addition, the thumb width was larger by 27%, giving a further mechanical advantage in the abduction/adduction axis. This is seen in Fig. 5A, where stiffness was increased in the abduction axis. In the hook axis, the stiffness was not seen to change substantially. This is in part due to the larger joint diameters reducing the curling behavior of the finger; therefore, the reduction in stiffness from this geometric effect opposed the increase in force transmission.

The aye-aye middle finger had the most extreme aspect ratio. The distance from the MCP to the tip was 7% longer, whereas the joint diameters were reduced by 56% and width was decreased by 51%, greatly reducing mechanical advantage. Therefore, we expected to see a reduction in finger stiffness. A low reduction was seen in the abduction axis because of friction already dominating the lowest stiffness behaviors. In the hook axis, the mean stiffness was reduced by 80%.

Thumb opposition is a substantial part of human manipulation capabilities, enabling greater in-hand dexterity and stability in various power grasps. To characterize the effect of the included opposition tendon (Fig. 3A) and to illustrate customizability of altering tendon arrangements, we performed additional stiffness characterization on the opposition axis of the human design. Tip force was measured in two postures, with the thumb adducted (opposition acts approximately in the abduction axis of the thumb) and with the thumb abducted (opposition acts approximately in the extension axis) (Fig. 5B). Compared with the abduction and extension axes of the MCP flexed index finger, stiffness was increased by a mean of 130%. Overall, we confirm that stiffness ranges are variable through joint diameters and bone lengths, allowing encoding at the design stage for passive interaction forces increasing up to 400% with the designs tested here.

Synergistic actuation mechanisms

The passive properties of OPH can be further extended to offer functional behaviors for active grasping and manipulation incorporating tendon actuation. In this section, we present three possible configurations of an actuation system whose goal is to complement and enhance the passive behaviors of the OPH. To maintain simplicity and accessibility, we limit the actuation up to two DoF. The performance of each configuration is characterized by the ability to modulate hand-environment interactions and transmit forces efficiently.

Actuation configurations

Figure 6A shows an overview of the modular actuation system that enables passive and active tendons to be routed to the hand. Passive tendons—those providing joint compression and finger restoring forces—were routed to a compact set of racks holding linear springs. Active tendons were routed to a mixer pulley. To ensure tension, these were routed through a series, nonlinear elastic system. This gives joint compliance and high force transmission when desired and enables an enhancement where the governing springs can be switched online to modulate relative tendon behaviors. We present three configurations of the modular actuation system in Fig. 6 (B to D), which offer increasing behavioral ranges.

Single-DoF actuation. Figure 6B shows the single pulley actuation system. This compact design connected the distal flexor tendon of each finger to a mixer pulley with stages' diameters scaled by the relative finger joint diameters (fig. S6A). The remaining tendons were connected to passive springs (fig. S5). Emerging from the base of the design is a single tendon. Thus, a single motor actuated this synergy to enable each finger to curl from an extended state to a palmar grasp (*49*). The passive behaviors could be further modified by changing the springs' stiffness and pre-tension (*70*). Pre-tension allows control over starting posture and choice of active tendon and mixer pulley diameters govern the final posture.

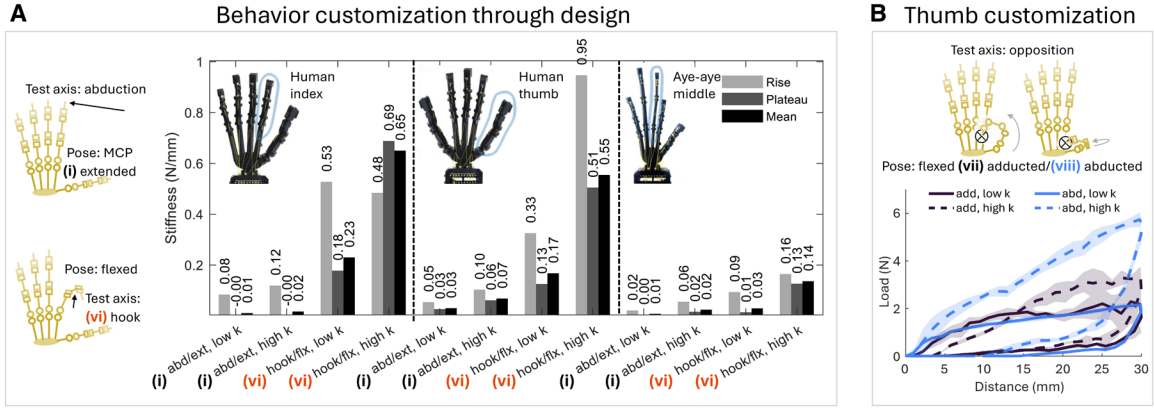

Fig. 5. Joint and finger stability and range of behavior with varying parametric designs. (**A**) Stiffness range in maximum (hook axis and flexed pose) and minimum stiffness axes (abduction axis and extended pose) with varied finger design. Up to 400% change in stiffness by varying finger design. (**B**) Additional tendons can be added to increase thumb opposition force/stiffness (mean and SD, $n = 3$).

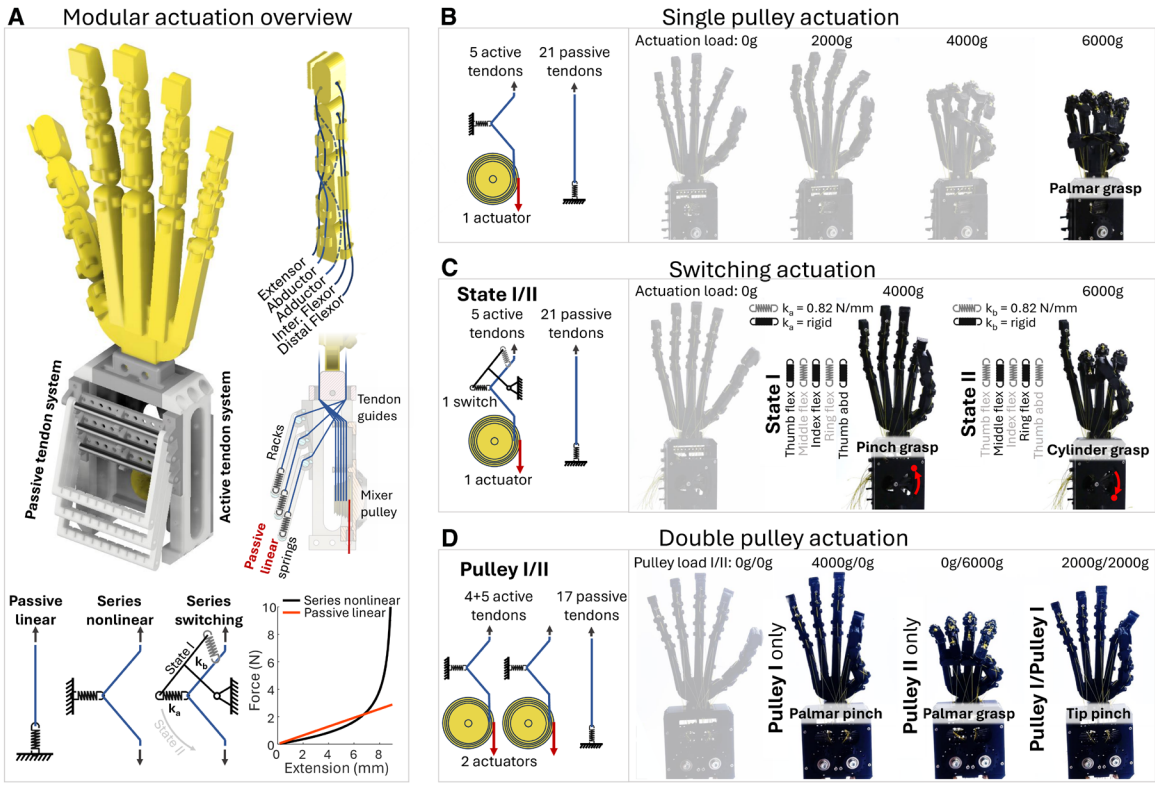

Fig. 6. Low degree of actuation for posture reconfiguration and behavior modulation. (**A**) Modular actuation overview. Twenty-six tendons must remain in tension: active tendons with series elasticity, passive tendons with linear springs. (**B**) Single-pulley actuation example: five active flexor tendons to form a palmar grasp type (*49*). (**C**) Switching actuation example modulates series stiffness with a lever: Five active tendons (thumb, index, middle and ring flexors, and thumb abductor) with switching spring configuration modulate between a pinch and cylinder grasp (state I/II). (**D**) Double-pulley actuation example: nine active tendons (four thumb/index flexors/add/abductors on pulley I and five flexors on pulley II) for two independent grasp types (palmar pinch/palmar grasp) and interpolations (for example: tip pinch).

Switching single-DoF actuation. By exploiting nonlinearities in the joint moment arm, tendon friction, and series elasticity and considering actuation as a modulation of underlying hand behaviors, a natural extension of the single pulley actuation system was to control spring properties online. Figure 6 (A and C) shows the schematic of this switchable stiffness mechanism: Each active tendon is routed through two series springs, and only one is active at a time depending on lever position. Five spring pairs simultaneously switch all tendons connected to the mixer pulley (fig. S6B). In the example routing, state I connects the thumb distal flexor, index distal flexor, and thumb abductor through rigid links (spring stiffness approximately infinite) and the middle and ring distal flexors through springs with 0.87-N/mm stiffness. The pre-tension of each active tendon is tuned to emphasize desired motions. State II inverts these stiffnesses. The effect is, in state I, that greater actuation force is transmitted to the thumb and index finger to form a precision pinch grasp (*49*) with high stiffness (Fig. 6C flex in the pinch grasp middle and ring finger are obscured by perspective). State II then relaxes the index and thumb and increases the middle and ring finger forces to form a more compliant pose resembling a power cylinder grasp. Therefore, behavior variation was seen with switching the position of a binary lever while externally actuating a single tendon.

Two-DoF actuation. A second approach to extending the behavioral range was to introduce additional parallel actuators. By incorporating two mixer pulleys, each independently actuated, multiple synergies can be generated and combined. Figure 6D shows the double-pulley actuation example. In this routing, each pulley actuates an independent set of tendons to generate different postures. The first pulley (I) connects to the intermediate flexors of the thumb and index finger in addition to the thumb abductor and the sixth thumb tendon connecting the proximal OPH thumb bone (equivalent to the metacarpal in human anatomy) to the index metacarpal. Activating this pulley pulls together the pads of the fingertips similar to a palmar pinch grasp (*49*). The second pulley (II) connects to the same set of distal flexor tendons as seen in the single pulley actuation example (fig. S6C). This actuation system was able to form a precision pinch grasp and a power enclosing grasp, and by actuating both degrees of actuation simultaneously, a distinct tip pinch grasp was observed.

Actuation behavior characteristics

The actuation system should complement the diverse behaviors of the OPH and allow for simple exploitation. To evaluate each configuration, we first observed blocked force capabilities in different test axes. This had a similar motivation to the stiffness tests in capturing behavioral diversity and understanding the interaction behavior of the fingers. We then characterized the switching configuration's ability to modulate interaction stiffness and the real effects this had on grasping performance. Last, we evaluated the grasping force transmission capabilities of each configuration.

Single-DoF actuation behaviors. Figure 7A shows the blocked force of the single pulley actuation system when tested in four positions

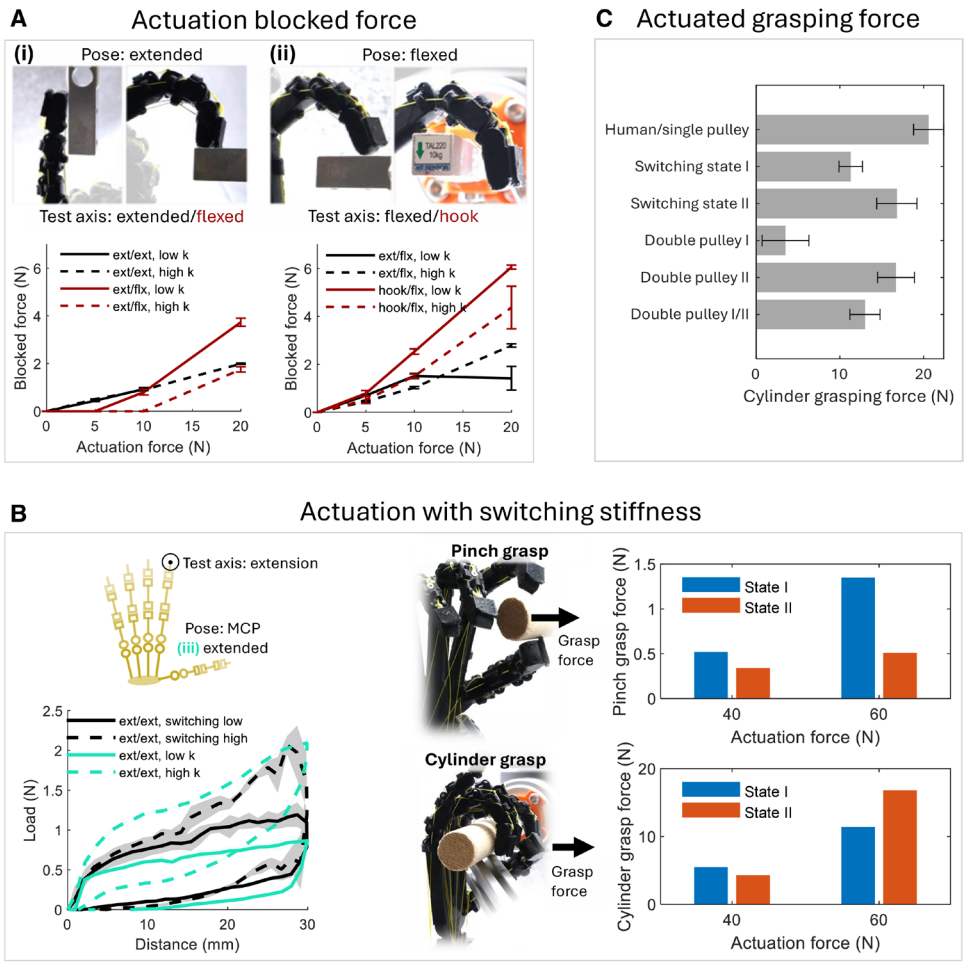

Fig. 7. Behavior range augmentation and modulation through actuation. (**A**) Finger force transmission range (mean and SD, $n = 3$). Tendon configuration and posture affect transmission efficiency. (**B**) Switching actuation results for an 80% change in finger stiffness with online control of spring switch state ($n = 3$). Switch states change pinch/cylinder grasping force performance to favor the state's posture. (**C**) Actuated grasping forces ($n = 3$). Grasping force is most efficient with single-pulley actuation, and there is lower efficiency with switching and double pulley, especially in pinch actuation modes.

from two starting postures and two spring configurations. Figure 7Ai shows the axes and results for starting in the extended position and measuring fingertip blocked force before deflection (in the extended position) and after (flexed). Figure 7Aii shows starting from a flexed position and measuring the force blocked at the fingertip and blocked at the PIP (hook).

Starting from the extended pose, the results in Fig. 7Ai show a linear behavior once contact was made between the finger and blocking load cell. When measuring from the extended position (black), this was immediate. When measuring from the MCP flexed position (red), contact occurred at 5- and 10-N loads for the low (solid line)– and high (dashed line)–stiffness passive spring configuration, respectively. In the stiffer spring configuration, to reach the MCP position, greater spring forces must be opposed. For high-actuation loads, a fingertip curling effect was seen (pose: extended and test axis: flexed), which led to the finger disengaging from the blocking load cell above 10 N.

In the flexed pose, Fig. 7Aii, the measured blocked force at the fingertip (black) dropped off at higher loads because of the finger curling and disengaging in the lower-stiffness configuration (solid line). The higher-stiffness passive tendons stabilized the finger and allowed greater force transmission even with higher antagonistic force. The force at the PIP joint (red) showed some nonlinear increase in blocked force with tendon load. This could be due to friction at lower actuation loads.

Switching mechanism behaviors. Figure 7B shows the characterization of the switching stiffness mechanism compared with the passive finger configuration in the extension axis (Fig. 4Ciii/iv). The switching state only modulates the stiffness of the distal flexor tendon compared with all five tendons of the passive configurations changing. Despite this, the switching mechanism had an increase in stiffness of 80% compared with 150%.

Figure 7B also shows a grasping force experiment with the two different switching states and two different grasp types measured. In the pinch grasp, a cylinder attached to a load cell, and the robot arm was positioned so, when the hand was actuated, the index finger and thumb contacted the cylinder. Grasping force was measured as the peak force when moving the cylinder with the robot arm away from the palm. In state I, the index and thumb distal flexor stiffness was greater, emphasizing the pinch grasp (Fig. 6C). This was reflected in

the grasping force results where, for both 40- and 60-N actuation forces, the grasping force in state I was higher.

The cylinder grasping force was measured identically to the pinch force, except the cylinder began closer to the palm for an enclosing grasp. The results (Fig. 7B cylinder) showed the maximum holding force in switching state II. With lower actuation force, state I grasping force was higher by 1.2 N; this was due to the high actuation force needed to flex all fingers into the fully enclosed posture of state II. The switching actuation overall behaved as intended, with each state showing favorable performance in the grasp type it was designed for at high actuation forces.

Comparison of actuation configuration behaviors. Figure 7C shows the grasping force experiment repeated on the human OPH design with the three example actuation configurations in their different operation modes. The single pulley actuation had the highest force, followed closely by switching state II and double pulley II (Fig. 6). This was expected because both modes were designed for power grasps, and the more complex tendon routing is likely less efficient at transmitting force. The pinch grasp–designed modes, switching I and double pulley I, had the lowest grasping force. In particular, double pulley I actuated only the intermediate rather than distal flexor tendons and so was able to transmit less force to the fingertips. Actuating both pulleys of the double-pulley example simultaneously (same total tendon load of 60 N) gave a holding force between either mode on its own given that the posture generated this way is also an interpolation.

Overall, we observed trade-offs in joint stability and force transfer with choice of passive spring configuration and in force transfer and actuation complexity with choice of active tendon configuration. The highest force performance was reached with fewer degrees of actuation. Therefore, the ability to customize synergies and generate the most diverse passive behaviors is critical for applications with broad task requirements and minimizing actuation.

Embodied manipulation with the OPH

We have so far demonstrated the flexibility in design and actuation in generating diverse and exploitable behaviors. In this section, we performed experiments to verify the utility of these behaviors and to explore how different performance metrics can be used to benchmark or optimize different hand designs. Last, we performed demonstrations to highlight the performance of different OPH designs and their unique manipulation behaviors.

Grasping performance

Figure 8A shows the results of an object grasping experiment with the three hand designs (movie S4) and three actuation examples. The mirrored hand with two thumbs and the aye-aye hand (Fig. 2B) were actuated with the single-pulley example using the mixer pulleys scaled to the relative joint diameters of each finger. All hands were controlled manually to allow exploration of diverse grasp types, and the variance introduced by manual operation was compensated for by coarse result grading: at least one stable grasp (object lifted, rotated, and placed down), at best an unstable weak grasp (object lifted but cannot be rotated without dropping), or the hand failing to form any grasp (fail to lift). Object properties are described in table S6.

Of the three hand designs, the mirrored human hand had the best performance in this manipulation set. The additional abducted thumb gave greater stability in grasping objects of similar size to the hand with more enclosure options; in particular, stable grasps formed readily during dynamic catching (Fig. 8A). The human hand design in the current configuration performed worse and was especially unable to grasp small objects because pinching motions could not be made. The aye-aye hand had the lowest overall performance, particularly struggling with the heavier compliant object and higher forces during dynamic catching. In these tests, grasps could often be formed, although they lacked the force to hold securely (compliant and thin). In others, the reduced opposability of the thumb restricted grasping (long and dynamic). However, this design had the best performance in grasping small objects, such as the 2-mm stalk of a strawberry (fine).

The last four rows of Fig. 8A show results of the three actuation systems. When allowing operation with both switching states or both of the double actuation pulleys, the human OPH completed the entire object-grasping set. Switching II and double pulley II both had similar performance to the single-pulley actuation of the human OPH, and as expected from the grasping force results (Fig. 7C), the pinch grasp actuation modes (switching I and double pulley II) had higher grasping stability for the smallest objects. The switching actuator performed better in this set of tasks, although minor differences in the two pinch-grasping types (Fig. 6, C and D) mean that the double-pulley system may perform better in a different task set.

Performance metrics

There is no comprehensive and compact dexterous manipulation or hand behavior benchmark (*71*). We defined our tests to highlight ranges of behaviors and the potential for dexterous capabilities important for accessible, customizable hands. We grounded this potential in comparisons with real human data (Fig. 4) and existing metrics such as grasp types (*49*) and precision manipulation (*65*). In Fig. 8B, we collated results from the above data for direct performance comparison with the metrics: object grasping performance, force, adaptability, reachability, and precision manipulation. For the actuation system comparison, reachability and precision manipulation were changed for active intersection and object redundancy. See the Supplementary Materials for full definitions of each.

The human and mirrored hand designs had similar performance (Fig. 8Bi) despite distinct grasp types in the object set. The aye-aye hand varied in force and adaptability. This arises from the high finger compliance and the largest reachability of all the designs, enabling many distinct grasp types for the object set despite a high failure rate. For precision manipulation, the human design was rated the highest; this should follow from our expectations from human hand evolution. The mirrored design had a slightly lower performance rating as a consequence of bias in the metric, where the measure does not account for previously unidentified modes enabled by this hand design, namely, that precise manipulation that could take place between the two thumbs.

Figure 8Bii shows performance metrics for the three actuation systems with the human OPH. Both the switching and double-pulley mechanism completed the object-grasp set, although they had lower force output from less efficient transmission. The adaptability was quantified by the maximum number of grasp types from a single actuation mode. Therefore, we saw that the double-pulley mechanism imposed a greater restriction on passive adaptability than the switching mechanism. The active intersection performed a similar role to the precision manipulation metric, in this case giving an indication of the particular manipulation workspaces enabled by the actuation modes. With more total active fingers in the double-pulley configuration, it scored the highest. Object redundancy captures the improved performance of

Fig. 8. Emergent manipulation behaviors and hand task space tuning. (**A**) Object manipulation set for adaptive whole-hand grasping. (**B**) Hands and actuation systems can be biased toward different ranges of applications. (**C**) Hand design unique capabilities: weight lifting and writing with the human hand, mirrored design multiobject grasping with sequential pinches, and aye-aye tree crawling and confined space manipulation.

individual actuation modes in the switching actuation compared with the double-pulley actuation. Overall, the actuation mechanism had a lower effect on performance than design variation, and the comparable performance of the two enhanced actuation modes was likely because of the similar choice of actuation synergies.

These metrics illustrate the competing requirements of dexterous hands and the tangible differences in performance and potential of varying morphologies and actuation. For general-purpose manipulation, these metrics were able to capture some performance information. However, more data are required to verify performance in a wider range of interactions, such as in-hand manipulation. For task-specific applications, key performance metrics are more easily selected and can be used as objective functions in different optimization algorithms. We see potential in multiobjective or diversity-based optimizations (*72*), unless the desired performance can be captured in a single metric. Then standard approaches such as Bayesian optimization can be used (fig. S2).

Emergent behaviors

Even with only a single degree of actuation, the three OPH designs exhibited diverse behavior ranges. With performance expectations from biological hand data (*43*, *62*) and intuition, we showcase unique manipulation demonstrations with each hand (movie S5).

With the human OPH, we performed a load test using the emergent high-strength hooking behavior (Fig. 4C) to lift up to 80 N (Fig. 8C). Load capacity was limited by slip from the hand overloading the actuation force, which is currently limited to 60 N by the strength of the actuation system. In addition, a writing demonstration was performed with the human hand design. Despite the lack of a frictional skin, the hand could hold a pen and write on paper with the same single-pulley actuation.

The mirrored hand design exhibited a unique pinch-grasping mode with the single-pulley actuation. With partial actuation, an object could be pinched between the thumbs, and then another pinch was formed between the remaining partially flexed fingers and the thumbs.

The aye-aye hand design was equipped with slender fingers for foraging inside confined spaces and arboreal locomotion (*56*). We demonstrated the ability to achieve stable grasping on branches and to operate in confined spaces by inserting the middle finger into the tree and retrieving an object, mimicking how aye-ayes use their fingers for the retrieval of insects.

DISCUSSION

Customizable hands have the potential to bridge the gap toward more general-purpose hands. With the ability to tune behaviors to a particular task space and leveraging compliant actuation, hands can be optimized for multitask applications. We saw this with the compliant grasping and rigid pinching behaviors exploiting nonlinear compliance in the OPH with switching and double-pulley actuation (Fig. 7B). We also began to see how morphology can influence task space with the varied capabilities of the human, mirrored, and aye-aye hand designs (Fig. 8). There remains substantial work in data collection over the design space outlined in Fig. 2A, particularly in investigating the complex morphology-manipulation skill mapping beyond object grasping and in discovery and selection of appropriate metrics for hand optimization. This is illustrated by paleoinspired robotics, where evolvable hardware can provide invaluable insights into the study of evolution, so long as capabilities are verified on extant species. The OPH is uniquely suited to exploring this design space through complex but tractable parameterization and rapid manufacturing capabilities.

Key to the OPH's success was the stability of low-level functionality and the diversity of emergent behaviors across varied parameterizations. We showed that the nonlinear, dislocatable, rolling joint has stable behaviors under high geometric variation and with high force capabilities. With joint ROM comparable to that of a real human finger, dynamic stiffness variation up to seven times (660% increase changing tendon configuration), and a further 400% stiffness variation through varying parameterization, interactions were effectively modulated to suit a variety of tasks. This was illustrated particularly in the high forces and varied grasp types seen in the human hand design, enabling grasping and writing with a pen, and compliance and delicate behaviors of the aye-aye design, particularly when interacting in confined spaces or adapting to different shapes (Fig. 8C). The second contribution was through the accessibility of the design. The single-piece printing capabilities with consumer-grade materials and a short bill of materials (≈30-g filament, bolts, and nylon tendons), along with the reconfigurable and simplified actuation, resulted in a more practical, low-cost design for large-scale real-world testing. There remains some complexity in the design of tendon configurations. Whether novice users find developing their own configurations intuitive or whether tools to derive custom actuation patterns are necessary is not yet known.

Substituting customization for dexterity does have limitations. Primarily, the task space of each individual hand will be limited when compared with dexterous hands, meaning the OPH fills a niche between single-task grippers and general-purpose dexterous hands. In addition, the current OPH design cannot reach the full manipulation space of a real hand; an 80-N holding force is high for robotic hands but low in comparison with humans. Design can be varied to increase holding force through larger joints and stiffer springs (Figs. 4 and 5), although this needs further exploration and actuation system optimization. Another limitation is the surface contact properties critical for fine manipulation skills and slip prevention. Introducing a parametric sensorized skin is an essential future step and should be done in a way that remains accessible, such as with silicone casting (*21*). These enhancements together would improve practicality for a number of real emerging applications, for example, high force ranges and robustness to uncertainties in flexible assembly; agriculture and social robotics (*52*, *53*, *73*); and lightweight, low-cost, and customizable functions/aesthetics for prosthetic applications (*51*).

Overall, the outcomes of our research demonstrate the potential of customizable hands in enhancing robotic manipulation versatility and performance. Inspired by the principles of human and primate anatomy and the flexibility of 3D printing, our findings could pave the way for the creation of more adaptable and efficient hands for multifunctional capabilities across a wide range of fields.

MATERIALS AND METHODS

Design objectives

Inspired by the varied manipulation capabilities observed across the primate taxonomy (*62*) and the desire to characterize embodiment in manipulation, we developed the OPH platform. The platform should be practical and accessible, for large-scale experimentation in the real world, while allowing for complex and emergent behaviors.

Considering the extensive demands of manipulation research, which involves repeated interactions with objects and environments, the design of our robotic hand prioritized robustness to endure prolonged real-world testing. Recognizing the limitations of research labs in achieving the reliability of commercially produced industrial products, we optimized the design for maximum durability of components and simplified repairs, including nylon tendons and reliefs along each tendon path for reduced friction. This approach not only accommodated the need for hundreds of hours of continuous experimentation without failure but also aligned with the capabilities of 3D printing and rapid prototyping technologies, making the skeletal designs of hands a resilient and practical tool for both industry and research settings.

Not included in the design objectives was control of tactile friction properties, palmar support, and isolation of tendons from external interactions. All of these are addressed with a skin. In addition, a fully enclosing skin allows for joint and tendon lubrication for more efficient force transmission and longer life (*19*). The best approach for implementation has not yet been found, whether through multimaterial printing, molding and casting, or manual assembly. The absence of a skin reduces performance, although it does not present any major problems to operation or investigation of behaviors. Therefore, we omitted the skin for future work.

Functional design features

The accessibility requirement constrains OPH design features to enable reliable fabrication with commercial 3D printers. Simplistic tendon pulleys that protrude rather than embed allow for ease of postprocessing, in the case of minor print defects, and ease of tendon

routing. Planar printing of pulleys and ligaments gives constraints on print angles and hand curvatures, especially if using fused deposition modeling (FDM) printing. For other technologies, such as selective laser sintering (SLS), with improved layer adhesion, this constraint can be relaxed. Smooth tendon paths with filleted surfaces improve force transmission but can increase overhanging surface angles and associated print defects; a balance has been found for reliable FDM printing.

Script-based parametric design

The open parametric design uses the open-source, script-based, computer-aided design (CAD) software OpenSCAD. The file structure follows the hierarchy of Fig. 3A. Modular joint and bone designs were assembled into fingers, which were, in turn, assembled into hands.

In current designs (Fig. 8), hand parameters are determined manually, for example, by measuring projected geometry (fig. S1). Pulley, ligament, and curvature parameters must be estimated from image, skeleton, or fossil data. Other methods exist for generating designs across the design space, each suited to different regions shown (Fig. 2A). Primate hand designs offer a predefined space with existing data we can exploit, either through exact replication or known examples or by generating hybrid or augmented designs by transferring defined characteristics or metrics (*45*). In our example (fig. S2A), we used key metrics from primates, the Napier indices, to create hybrid hand designs. Generative design exploiting large language models is an emerging field showing promise in capturing design intuition for nonexpert users (*47*), either through prompt engineering for formatted hand designs or more simply generating design briefs and converting to parameters (fig. S2B). Our third method, which reflects the natural development/evolution quadrant of Fig. 2A, is scaling or matching to a human. With interest in accessible and personalized prosthetics (*54*), the OPH design can be automatically generated with landmark extraction algorithms such as MediaPipe (*63*) (fig. S2C). A final example is design through metric-based optimization. Bayesian optimization is one such approach suited for moderate numbers of parameters and complex objective functions. We show a number of examples where Bayesian optimization was implemented using the Matlab Statistics and Machine Learning Toolbox and objective functions of reciprocal reachability volumes (fig. S2D). Reachability volumes have been selected because they reflect different manipulation tasks and typically should be maximized for versatile manipulation. Figure S2D provides four examples that increase in complexity, where the number of parameters optimized increases from 3 (finger bone lengths with fourth constrained) to 21 (15 bone lengths and six angles).

Modular actuation: Single pulley

The single-pulley actuation example allows for up to 30 passively connected tendons and five active tendons in a single synergy. In Fig. 6B, the five active tendons are the distal flexor tendon of each finger through the series elastic mechanism with 0.87-N/mm springs (fig. S6A). For the thumb, middle, index, ring, and little finger, the pulley radius is scaled by joint diameter: 21.0, 19.4, 18.3, 18.3, and 16.0 mm, respectively. The remaining tendons are routed to the passive spring racks with a stiffness of 0.32 N/mm (intermediate flexor and extensor) or 0.11 N/mm (abductor and adductor). This follows the default spring configuration (fig. S5).

Modular actuation: Stiffness switching

The switching stiffness follows the same design and principles as the single-pulley version. Additional space is needed for the switching system, which mounts a pair of springs for each of the five active tendons (Fig. 6C). Each tendon path is offset around the lever point of rotation such that, in one state, only one of the spring pair at a time is coupled to the tendon force/extension. In the configuration shown in Fig. 6C, the five active tendons are the distal flexor of the thumb, middle, index, and ring finger and the thumb abductor, with mixer pulley radii of 21.0, 19.4, 18.3, 18.3, and 16.0 mm, respectively. In the first state, the two thumb tendons and the index flexor are coupled through rigid "springs." In the second state, these tendons are coupled to 0.87-N/mm springs. The middle and ring tendons have the opposite configuration. Passive tendons were configured as with the single-pulley version.

Modular actuation: Double pulley

The double-pulley system was configured to operate on two independent sets of tendons. The first pulley connects the thumb and index intermediate flexors and the thumb abductor and adductor. By actuating both abductor and adductor with nonlinear series springs, the joint stiffness was increased, allowing for greater opposition and pinching force. The second pulley mirrors the single pulley actuation. For both pulleys, 0.87-N/mm springs were used in series, and passive tendons were configured as with the single-pulley version.

Fabrication and assembly

The hand and actuation systems were designed for 3D printing. FDM is the most accessible, although it introduces a higher chance of print defects compared with SLS or stereolithography (SLA) printing. Three hands were printed for this work (Fig. 2B), each using a Prusa MK3 printer and polypropylene filament. Design parameters were extracted from skeletal diagrams and scaled to a maximum finger length of 150 mm. The hands were printed in 6 to 9 hours with the only postprocessing being support material removal and routing of tendons through pulleys to their respective anchor points (Fig. 4B). We identified nylon or polyamide as alternative materials with desirable properties that can be printed via FDM or SLS.

The actuation systems have optimizations for reducing manufacturing time, for example, tendon clips for rapid spring attachment and tuning of tension (fig. S5), pivoting racks for access to assemble and tune the dense passive array, and tendons routed through rigid pulley points to reduce part count (Fig. 6A). With the exception of mixer pulley bearings and smooth rods for three low-friction-bearing surfaces and fasteners, the entire actuation box was 3D printed using standard materials such as polylactic acid (PLA). After assembling the actuation box with fasteners, each tendon was routed through up to two internal pulley points to either passive springs or mixer pulley. Assembly is straightforward, albeit repetitive.

Experimental setup

We characterized the parametric design at three levels: first, the low-level joint and finger ranges of behavior. Second, we characterized the behavioral range and stability over varying hand parameterization. Third, we tested the hands fully integrated with actuation to observe overall performance and emergent behaviors.

In the first set of experiments, a single finger configuration was varied. For ROM, tendon pre-tensions were adjusted manually, and angle changes were measured by image data. During stiffness testing, a UR5 robot arm equipped with a load cell probed the finger in various test axes while the finger was affixed to a table (Fig. 4C and fig. S4). Displacement was recorded by robot position, and force was recorded directly from the calibrated load cell. Force was sampled, loading and unloading the fingers, in 0.5-mm intervals. Three repeats were performed, and results are shown in Figs. 4C, 5, and 7B.

The second set of experiments repeated the above setup with three different finger designs (Fig. 5A). An additional experiment was performed with the thumb augmented with an opposition tendon connected to a 0.32-N/mm spring (low stiffness) or 0.87-N/mm spring (high stiffness).

The third set of tests, augmented with actuation, measured blocked force, switching stiffness change, and grasping forces similarly using a UR5-mounted load cell (Fig. 7). During blocked force, the single actuation tendon was loaded with successive weights rather than the load cell probing. During switching stiffness, rather than tendons being reconfigured manually, just the lever was switched. During grasping, a dowel was attached to the load cell for grip with the whole hand (Fig. 7B).

The relative performance of the different hand designs and actuation system examples was lastly explored with an object-grasping test. The hands were equipped with 3D printed manual handles for motion and actuation directly from a user (Fig. 8C). Objects were chosen to represent size and shape changes with regular spheres and cylinders. Additional objects were chosen for compliant, dynamic, and delicate grasping. Each test was performed attempting to pick up the object from a flat surface, rotate it, and replace it on the surface, except for the dynamic test where the object began in the hand and then must be thrown and caught.

Statistical analysis

In Figs. 4C, 5B, and 7 (A to C), presented data were calculated from the mean and SD (sample) with $n = 3$. In Fig. 8B, metrics were calculated with mean results ($n = 3$) or derived data (reported in the Supplementary Materials).

Supplementary Materials

The PDF file includes:

Methods
Legends for movies S1 to S5
Figs. S1 to S6
Tables S1 to S6
Reference (*74*)

Other Supplementary Material for this manuscript includes the following:

Movies S1 to S5

REFERENCES AND NOTES

1. C. Piazza, G. Grioli, M. G. Catalano, A. Bicchi, A century of robotic hands. *Annu. Rev. Control Robot. Auton. Syst.* **2**, 1–32 (2019).
2. S. Puhlmann, J. Harris, O. Brock, RBO hand 3: A platform for soft dexterous manipulation. *IEEE Trans. Robot.* **38**, 3434–3449 (2022).
3. J. Hughes, U. Culha, F. Giardina, F. Guenther, A. Rosendo, F. Iida, Soft manipulators and grippers: A review. *Front. Robot. AI* **3**, 69 (2016).
4. M. Wilson, Six views of embodied cognition. *Psychon. Bull. Rev.* **9**, 625–636 (2002).
5. A. Clark, *Being There: Putting Brain, Body, and World Together Again* (MIT Press, 1998).
6. M. W. Marzke, K. L. Wullstein, Chimpanzee and human grips: A new classification with a focus on evolutionary morphology. *Int. J. Primatol.* **17**, 117–139 (1996).
7. S. J. Edwards, J. D. McCoy-Powlen, D. Gallen, M. A. Suarez, *Hand Grasps and Manipulation Skills: Clinical Perspective of Development and Function* (Routledge, 2024).
8. R. Pfeifer, M. Lungarella, F. Iida, Self-organization, embodiment, and biologically inspired robotics. *Science* **318**, 1088–1093 (2007).
9. K. Gilday, J. Hughes, F. Iida, Sensing, actuating, and interacting through passive body dynamics: A framework for soft robotic hand design. *Soft Robot.* **10**, 159–173 (2023).
10. Y. Liu, Z. Li, H. Liu, Z. Kan, B. Xu, Bioinspired embodiment for intelligent sensing and dexterity in fine manipulation: A survey. *IEEE Trans. Industr. Inform.* **16**, 4308–4321 (2020).
11. I. Akkaya, M. Andrychowicz, M. Chociej, M. Litwin, B. M. Grew, A. Petron, A. Paino, M. Plappert, G. Powell, R. Ribas, J. Schneider, N. Tezak, J. Tworek, P. Welinder, L. Weng, Q. Yuan, W. Zaremba, L. Zhang, Solving Rubik's cube with a robot hand. arXiv:1910.07113 [cs.LG] (2019).
12. X. Pan, A. Garg, A. Anandkumar, Y. Zhu, "Emergent hand morphology and control from optimizing robust grasps of diverse objects," in *2021 IEEE International Conference on Robotics and Automation (ICRA)* (IEEE, 2021), pp. 7540–7547.
13. I. M. Bullock, A. M. Dollar, "Classifying human manipulation behavior," in *2011 IEEE International Conference on Rehabilitation Robotics* (IEEE, 2011), pp. 1–6.
14. Y. Kim, Z. Pan, K. Hauser, "Mo-bbo: Multi-objective bilevel bayesian optimization for robot and behavior co-design," in *2021 IEEE International Conference on Robotics and Automation (ICRA)* (IEEE, 2021), pp. 9877–9883.
15. E. Mattar, A survey of bio-inspired robotics hands implementation: New directions in dexterous manipulation. *Rob. Auton. Syst.* **61**, 517–544 (2013).
16. Shadow Robot Company, Dexterous hand series (2024); https://shadowrobot.com/dexterous-hand-series/.
17. M. Grebenstein, M. Chalon, W. Friedl, S. Haddadin, T. Wimböck, G. Hirzinger, R. Siegwart, The hand of the DLR hand arm system: Designed for interaction. *Int. J. Rob. Res.* **31**, 1531–1555 (2012).
18. Z. Xu, E. Todorov, "Design of a highly biomimetic anthropomorphic robotic hand towards artificial limb regeneration," in *2016 IEEE International Conference on Robotics and Automation (ICRA)* (IEEE, 2016), pp. 3485–3492.
19. Y.-J. Kim, J. Yoon, Y.-W. Sim, Fluid lubricated dexterous finger mechanism for human-like impact absorbing capability. *IEEE Robot. Autom. Lett.* **4**, 3971–3978 (2019).
20. A. D. Deshpande, Z. Xu, M. J. V. Weghe, B. H. Brown, J. Ko, L. Y. Chang, D. D. Wilkinson, S. M. Bidic, Y. Matsuoka, Mechanisms of the anatomically correct testbed hand. *IEEE/ASME Trans. Mechatron.* **18**, 238–250 (2013).
21. K. Gilday, T. George-Thuruthel, F. Iida, Predictive learning of error recovery with a sensorized passivity-based soft anthropomorphic hand. *Adv. Intell. Syst.* **5**, 2200390 (2023).
22. M. G. Catalano, G. Grioli, E. Farnioli, A. Serio, C. Piazza, A. Bicchi, Adaptive synergies for the design and control of the Pisa/IIT SoftHand. *Int. J. Robot. Res.* **33**, 768–782 (2014).
23. C. Della Santina, C. Piazza, G. Grioli, M. G. Catalano, A. Bicchi, Toward dexterous manipulation with augmented adaptive synergies: The Pisa/IIT SoftHand 2. *IEEE Trans. Robot.* **34**, 1141–1156 (2018).
24. K. Junge, J. Hughes, Robust anthropomorphic robotic manipulation through biomimetic distributed compliance. arXiv:2404.05262 [cs.RO] (2024).
25. J. Park, M. Chang, I. Jung, H. Lee, K. Cho, 3D printing in the design and fabrication of anthropomorphic hands: A review. *Adv. Intell. Syst.* **6**, 2300607 (2024).
26. H. Lee, J. Park, B. B. Kang, K.-J. Cho, Single-step 3D printing of bio-inspired printable joints applied to a prosthetic hand. *3D Print. Addit. Manuf.* **10**, 917–929 (2023).
27. L. Tian, N. Magnenat-Thalmann, D. Thalmann, J. Zheng, "A methodology to model and simulate customized realistic anthropomorphic robotic hands," in *Proceedings of Computer Graphics International 2018* (Association for Computing Machinery, 2018), pp. 153–162.
28. A. Mohammadi, J. Lavranos, H. Zhou, R. Mutlu, G. Alici, Y. Tan, P. Choong, D. Oetomo, A practical 3D-printed soft robotic prosthetic hand with multiarticulating capabilities. *PLOS ONE* **15**, e0232766 (2020).
29. A. Mohammadi, J. Lavranos, Y. Tan, P. Choong, D. Oetomo, "A paediatric 3D-printed soft robotic hand prosthesis for children with upper limb loss," in *2020 42nd Annual InternationalConference of the IEEE Engineering in Medicine & Biology Society (EMBC)* (IEEE, 2020), pp. 3310–3313.
30. R. Deimel, P. Irmisch, V. Wall, O. Brock, "Automated co-design of soft hand morphology and control strategy for grasping," in *2017 IEEE/RSJ International Conference on Intelligent Robots and Systems (IROS)* (IEEE, 2017), pp. 1213–1218.
31. P. Mannam, X. Liu, D. Zhao, J. Oh, N. Pollard, "Design and control co-optimization for automated design iteration of dexterous anthropomorphic soft robotic hands," in *2024 IEEE 7th International Conference on Soft Robotics (RoboSoft)* (IEEE, 2024), pp. 332–339.
32. C. Tawk, H. Zhou, E. Sariyildiz, M. in het Panhuis, G. M. Spinks, G. Alici, Design, modeling, and control of a 3D printed monolithic soft robotic finger with embedded pneumatic sensing chambers. *IEEE/ASME Trans. Mechatron.* **26**, 876–887 (2020).
33. G. Bai, N. Rojas, "Self-adaptive monolithic anthropomorphic finger with teeth-guided compliant cross-four-bar joints for underactuated hands," in *2018 IEEE-RAS 18th International Conference on Humanoid Robots (Humanoids)* (IEEE, 2018), pp. 145–152.
34. J. Hughes, P. Maiolino, F. Iida, An anthropomorphic soft skeleton hand exploiting conditional models for piano playing. *Sci. Robot.* **3**, eaau3098 (2018).

35. T. Buchner, S. Weirich, A. M. Kübler, W. Matusik, R. K. Katzschmann, "Replicating human anatomy with vision controlled jetting–a pneumatic musculoskeletal hand and forearm," in *2024 IEEE 7th International Conference on Soft Robotics (RoboSoft)* (IEEE, 2024), pp. 183–189.
36. J. T. Belter, J. L. Segil, A. M. Dollar, R. F. Weir, Mechanical design and performance specifications of anthropomorphic prosthetic hands: A review. *J. Rehabil. Res. Dev.* **50**, 599–618 (2013).
37. J. Lázaro-Guevara, R. Gondokaryono, L. González, K. Garrido, N. Sujumnong, A. Wee, J. Miscione, A graphic user interface (GUI) to build a cost-effective customizable 3D printed prosthetic hand. bioRxiv 2020.03.18.997486 [Preprint] (2020). https://doi.org/10.1101/2020.03.18.997486.
38. R. R. Ma, L. U. Odhner, A. M. Dollar, "A modular, open-source 3d printed underactuated hand," in *2013 IEEE International Conference on Robotics and Automation* (IEEE, 2013), pp. 2737–2743.
39. D. Bauer, C. Bauer, A. Lakshmipathy, R. Shu, N. S. Pollard, "Towards very low-cost iterative prototyping for fully printable dexterous soft robotic hands," in *2022 IEEE 5th International Conference on Soft Robotics (RoboSoft)* (IEEE, 2022), pp. 490–497.
40. D. Lim, T. Georgiou, A. Bhardwaj, G. D. O'Connell, A. M. Agogino, "Customization of a 3D printed prosthetic finger using parametric modeling," in *International Design Engineering Technical Conferences and Computers and Information in Engineering Conference* (American Society of Mechanical Engineers, 2018), vol. 51753, p. V02AT03A034.
41. R. Paz, E. Pei, M. Monzón, F. Ortega, L. Suárez, Lightweight parametric design optimization for 4D printed parts. *Integr. Comput. Aided Eng.* **24**, 225–240 (2017).
42. J. Xu, T. Chen, L. Zlokapa, M. Foshey, W. Matusik, S. Sueda, P. Agrawal, An end-to-end differentiable framework for contact-aware robot design. arXiv:2107.07501 [cs.RO] (2021).
43. P. Kieliba, D. Clode, R. O. Maimon-Mor, T. R. Makin, Robotic hand augmentation drives changes in neural body representation. *Sci. Robot.* **6**, eabd7935 (2021).
44. D. M. Fragaszy, J. Crast, "Functions of the hand in primates," in *The Evolution of the Primate Hand: Anatomical, Developmental, Functional, and Paleontological Evidence* (Springer, 2016), pp. 313–344.
45. J. R. Napier, P. H. Napier, *A Handbook of Living Primates: Morphology, Ecology and Behaviour of Nonhuman Primates* (Academic Press, 1967).
46. V. Perricone, T. Grun, P. Raia, C. Langella, Paleomimetics: A conceptual framework for a biomimetic design inspired by fossils and evolutionary processes. *Biomimetics* **7**, 89 (2022).
47. F. Stella, C. Della Santina, J. Hughes, How can LLMs transform the robotic design process? *Nat. Mach. Intell.* **5**, 561–564 (2023).
48. T. Chen, Z. He, M. Ciocarlie, Co-designing hardware and control for robot hands. *Sci. Robot.* **6**, eabg2133 (2021).
49. T. Feix, J. Romero, H.-B. Schmiedmayer, A. M. Dollar, D. Kragic, The grasp taxonomy of human grasp types. *IEEE Trans. Hum. Mach. Syst.* **46**, 66–77 (2015).
50. J. Napier, The evolution of the hand. *Sci. Am.* **207**, 56–65 (1962).
51. F. Cordella, A. L. Ciancio, R. Sacchetti, A. Davalli, A. G. Cutti, E. Guglielmelli, L. Zollo, Literature review on needs of upper limb prosthesis users. *Front. Neurosci.* **10**, 209 (2016).
52. G. Rosati, M. Faccio, A. Carli, A. Rossi, Fully flexible assembly systems (F-FAS): A new concept in flexible automation. *Assembly Autom.* **33**, 8–21 (2013).
53. B. Zhang, Y. Xie, J. Zhou, K. Wang, Z. Zhang, State-of-the-art robotic grippers, grasping and control strategies, as well as their applications in agricultural robots: A review. *Comput. Electron. Agric.* **177**, 105694 (2020).
54. E. Biddiss, D. Beaton, T. Chau, Consumer design priorities for upper limb prosthetics. *Disabil. Rehabil. Assist. Technol.* **2**, 346–357 (2007).
55. A. Saikia, S. Mazumdar, N. Sahai, S. Paul, D. Bhatia, S. Verma, P. K. Rohilla, Recent advancements in prosthetic hand technology. *J. Med. Eng. Technol.* **40**, 255–264 (2016).
56. E. J. Sterling, E. E. McCreless, "Adaptations in the aye-aye: A review," in *Lemurs: Ecology and Adaptation*, L. Gould, M. L. Sauther, Eds. (Springer, 2006), pp. 159–184.
57. T. R. Makin, F. de Vignemont, S. Micera, Soft embodiment for engineering artificial limbs. *Trends Cogn. Sci.* **24**, 965–968 (2020).
58. A. Minami, K.-N. An, W. P. Cooney III, R. L. Linscheid, E. Y. Chao, Ligamentous structures of the metacarpophalangeal joint: A quantitative anatomic study. *J. Orthop. Res.* **1**, 361–368 (1983).
59. A. Amis, M. Jones, The interior of the flexor tendon sheath of the finger. the functional significance of its structure. *J. Bone Joint Surg. Br.* **70**, 583–587 (1988).
60. C. Bell, *The Hand: Its Mechanism and Vital Endowments, as Evincing Design*, vol. 4 (Bell & Daldy 1865).
61. T. D. White, B. Asfaw, Y. Beyene, Y. Haile-Selassie, C. O. Lovejoy, G. Suwa, G. WoldeGabriel, *Ardipithecus ramidus* and the paleobiology of early hominids. *Science* **326**, 64–86 (2009).
62. S. Almécija, C. Sherwood, "Hands, brains, and precision grips: Origins of tool use behaviors," in *The Nervous Systems of Non-Human Primates*, L. Krubitzer, Ed., vol. 3 of *Evolution of Nervous Systems*, J. H. Kaas, Ed. (Academic Press, 2017), pp. 299–315.
63. F. Zhang, V. Bazarevsky, A. Vakunov, A. Tkachenka, G. Sung, C.-L. Chang, M. Grundmann, Mediapipe hands: On-device real-time hand tracking. arXiv:2006.10214 [cs.CV] (2020).
64. O. Porges, T. Stouraitis, C. Borst, M. A. Roa, "Reachability and capability analysis for manipulation tasks," in *ROBOT2013: First Iberian Robotics Conference: Advances in Robotics*, vol. 2 (Springer, 2014), pp. 703–718.
65. I. M. Bullock, T. Feix, A. M. Dollar, Workspace shape and characteristics for human two and three-fingered precision manipulation. *IEEE Trans. Biomed. Eng.* **62**, 2196–2207 (2015).
66. G. Cotugno, K. Althoefer, T. Nanayakkara, The role of the thumb: Study of finger motion in grasping and reachability space in human and robotic hands. *IEEE Trans. Syst. Man Cybern. Syst.* **47**, 1061–1070 (2016).
67. A. De, U. Tasch, A two-DOF manipulator with adjustable compliance capabilities and comparison with the human finger. *J. Robot. Syst.* **13**, 25–34 (1996).
68. B. Vanderborght, A. Albu-Schaeffer, A. Bicchi, E. Burdet, D. G. Caldwell, R. Carloni, M. Catalano, O. Eiberger, W. Friedl, G. Ganesh, M. Garabini, M. Grebenstein, G. Grioli, S. Haddadin, H. Hoppner, A. Jafari, M. Laffranchi, D. Lefeber, F. Petit, S. Stramigioli, N. Tsagarakis, M. van Damme, R. van Ham, L. C. Visser, S. Wolf, Variable impedance actuators: A review. *Rob. Auton. Syst.* **61**, 1601–1614 (2013).
69. A. Z. Hajian, R. D. Howe, Identification of the mechanical impedance at the human finger tip. *J. Biomech. Eng.* **119**, 109–114 (1997).
70. K. Gilday, J. Hughes, F. Iida, Wrist-driven passive grasping: Interaction-based trajectory adaption with a compliant anthropomorphic hand. *Bioinspir. Biomim.* **16**, 026024 (2021).
71. K. Gilday, F. Iida, "Intelligent soft hands and benchmarking towards general-purpose robotic manipulation," in *IOP Conference Series: Materials Science and Engineering*, vol. 1261 (IOP Publishing, 2022), p. 012010.
72. J. Pinskier, X. Wang, L. Liow, Y. Xie, P. Kumar, M. Langelaar, D. Howard, Diversity-based topology optimization of soft robotic grippers. *Adv. Intell. Syst.* **6**, 2300505 (2024).
73. C. Blanes, M. Mellado, C. Ortiz, A. Valera, Technologies for robot grippers in pick and place operations for fresh fruits and vegetables. *Span. J. Agric. Res.* **9**, 1130–1141 (2011).
74. L. Tian, J. Zheng, Y. Cai, M. F. K. Bin Abdul Halil, N. M. Thalmann, D. Thalmann, H. Li, Fast 3D modeling of prosthetic robotic hands based on a multi-layer deformable design. *Int. J. Bioprint.* **8**, 406 (2022).

Acknowledgments

Funding: This work was supported by the European Union's Horizon 2020 research and innovation programme under the Marie Skłodowska-Curie grant agreement no. 101034260 and SNSF project funding no. 200021_215030. **Author contributions:** K.G. conceptualized, designed, and performed all experiments and wrote the paper. C.S. conceptualized and wrote the paper. F.I. conceptualized and proofread the paper. J.H. provided funding and conceptualized and wrote the paper. **Competing interests:** The authors declare that they have no competing interests. **Data and materials availability:** All data needed to evaluate the conclusions in the paper are present in the paper and/or the Supplementary Materials. The data for this study have been deposited in the database doi.org/10.5281/zenodo.13362060. Source files for the OPH can be found here: doi.org/10.5281/zenodo.15210918.

Submitted 31 August 2024
Accepted 17 April 2025
Published 14 May 2025
10.1126/scirobotics.ads6437

Science Robotics

Embodied manipulation with past and future morphologies through an open parametric hand design

Kieran Gilday, Chapa Sirithunge, Fumiya Iida, and Josie Hughes

Sci. Robot. **10** (102), eads6437. DOI: 10.1126/scirobotics.ads6437

Science Robotics (ISSN 2470-9476) is published by the American Association for the Advancement of Science. 1200 New York Avenue NW, Washington, DC 20005. The title *Science Robotics* is a registered trademark of AAAS.